ACS APPLIED MATERIALS & INTERFACES

www.acsami.org

Research Article

Millimeter-Wave and Short-Range Wireless Communication Antenna Based on High-Conductivity Graphene-Assembled Film

Yitong Xin,[⊥] Rongguo Song,*[,⊥] Shaoqiu Jiang, Huaqiang Fu, Wei Qian, Dong Ye, Jiannan Guo, Zixin Zhang, Haoran Zu,* and Daping He*

Cite This: https://doi.org/10.1021/acsami.3c10732

Read Online

ACCESS | Metrics & More | Article Recommendations | Supporting Information

ABSTRACT: Millimeter-wave and short-range wireless communication is an important part of the Internet of Things due to its advantages of high transmission speed and large data capacity. In this paper, two antenna arrays operating at typical millimeter-wave bands (45 and 60 GHz) based on graphene-assembled films (GAF) are proposed for short-range wireless communication application. The 45 GHz graphene-assembled film antenna array is in the form of a magnetoelectric dipole antenna with a strip slot coupling to achieve bidirectional radiation, which offers an operating bandwidth of 40−49.5 GHz with a realized gain of 11.8 dBi. The 60 GHz graphene-assembled film antenna utilizes a microstrip discontinuous radiation array to achieve radiation with an operating bandwidth of 59−64 GHz, reaching the peak realized gain of 14.92 dBi over the working frequency. Finally, we proposed an experimental validation to verify the transmission performance of both antenna arrays in an actual conference room. The results show that the signal drops slowly in the room with drop rates of 0.064 dB/cm (at 45 GHz) and 0.071 dB/cm (at 60 GHz), while it steeply dropped through the wall with the drop rates of 2.3 and 3.13 dB/cm, more than 35-fold difference in signal drop rates in the room and through the wall. It has been confirmed that the proposed antenna arrays can successfully realize fast indoor short-range wireless communication while also preventing signal leakage through walls, thereby enhancing the security of information. In summary, this is the first time that we have applied graphene-based materials to millimeter-wave and short-range wireless communications, revealing the significant potential of carbon-based materials in high-frequency communication systems.

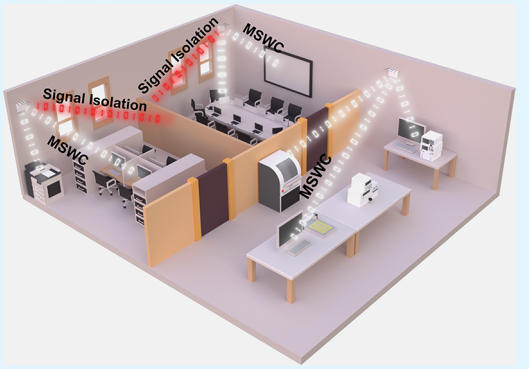

KEYWORDS: *graphene-assembled film, millimeter wave, short-range wireless communication, antenna array, signal safety*

1. INTRODUCTION

Nowadays, more and more high-data transmission applications are emerging in daily life, such as high-definition television, autopilot, and augmented reality/virtual reality.[1−3] Therefore, typical millimeter-wave bands for short-range wireless communication have been put forward, such as the 45 GHz band (IEEE 802.11aj) and 60 GHz band (IEEE 802.11ad),[4,5] which are worldwide license-free, providing the foundation for high-speed wireless communication.[6,7] Millimeter-wave wireless communication usually requires the antennas to be miniaturized and of wide bandwidth and high gain.[8−11] In addition, with the environment in which antennas operate becoming more and more complex, the explosive growth of antennas and other electronics also puts forward higher requirements for conductive materials. In the past, traditional metal materials such as copper, aluminum, and gold were extensively used for the manufacture of electronic devices, which led to environmental issues due to the pollution from the electronic waste.[12,13] In the meantime, the existing millimeter-wave antennas are mostly copper-based, making it difficult to obtain them with corrosion resistance, lightweight, and environmental friendliness to face the increasingly complex and versatile application scenarios.[14−16] Therefore, it is urgent to explore new-generation materials for application in millimeter-wave short-range wireless communication (MSWC), which can ensure the good working performance of electronic devices while possessing excellent mechanical stability, chemical stability, and environmental benignancy.

Graphene-based materials are considered to be the most excellent substitutes for metal materials.[17] The application of macro-graphene-based materials has been the hotspot in the field of electronic devices, such as RFID antennas and microwave antennas.[18−20] However, the graphene-based films, limited by the low conductivity (below 10^5 S/m) and low accuracy of the printing process,[21−23] lead to significant

Received: July 21, 2023
Revised: November 1, 2023
Accepted: November 2, 2023

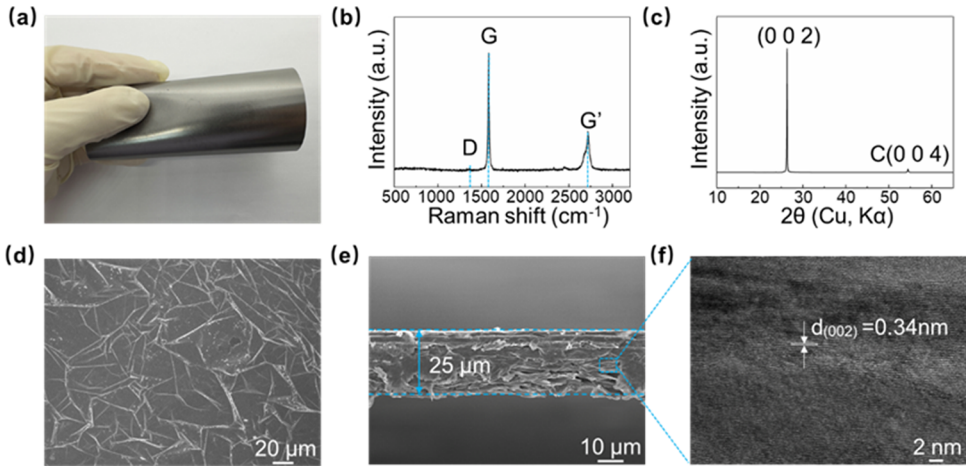

Figure 1. Characterization of graphene-assembled films (GAFs). (a) Typical photograph of the GAF. (b) Raman spectra of the GAF. (c) X-ray diffraction patterns of the GAF. (d) Typical scanning electron microscopy (SEM) image of the GAF surface. (e) Typical SEM image of the GAF cross section. (f) Typical high-resolution transmission electron microscopy (HRTEM) image of the GAF cross section.

losses and sharp deterioration of performance in the millimeter-wave band. In our previous work, highly conductive (10^6 S/m) graphene-assembled films (GAFs) were proposed and prepared,[24] which have mechanical stability, corrosion resistance, and thermal conductivity far superior to that of metals while maintaining similar electrical properties, making high-performance millimeter-wave graphene-based film antennas possible. GAF has been successfully applied to radio-frequency devices such as antennas, filters, and metasurfaces.[25−27] Further, we are also working on developing various types of GAF 5G millimeter-wave and long-range wireless antennas.[28−30] All the GAF-based antennas show excellent corrosion resistance, environmental friendliness, and lightweight. However, the existing GAF antennas are mostly concentrated in the low-frequency band (below 30 GHz), and high-frequency millimeter-wave short-range wireless communication has not been reported.

In this work, we present a 45 GHz magnetoelectric dipole antenna array based on GAF, which provides a 40−50 GHz operating bandwidth and 11.8 dBi of peak realized gain. The proposed 45 GHz antenna array offers bidirectional symmetric radiation in the *xoz*-plane with a half-power beamwidth of 16°. To apply GAF to higher frequency bands, we further demonstrate a 60 GHz GAF microstrip discontinuous radiation antenna array. The proposed 60 GHz antenna array has an operating bandwidth of 59−64 GHz with a peak realized gain of 14.92 dBi and a half-power beamwidth of 9° in the *xoz*-plane. Furthermore, to verify the performance of the indoor short-range communication, we construct a wireless communication scheme for signal transfer in an actual conference room. These results display that in the room the signal drops slowly to −27 and −30 dB (0.064 dB/cm at 45 GHz and 0.071 dB/cm at 60 GHz), while through the wall the signal drops precipitously to −60 and −77 dB at rates of 2.3 and 3.13 dB/cm, respectively. The proposed antenna arrays have signal coverage for the entire room and restrain the signal leakage through the wall, showing great application values for future millimeter-wave short-range wireless communication with signal safety.

2. METHOD OF GAF PREPARATION

A highly conductive GAF is fabricated by secondary high-temperature annealing.[24] First, the graphene oxide (GO) suspension (15 mg/mL) was scraped onto a polyethylene terephthalate (PET) substrate and dried at a temperature of 70−80 °C to produce GO films. Second, the GO films were annealed at 1300 °C for 2 h and under argon (Ar) atmosphere at 2850 °C for 1 h. Then, the single-layer annealed graphene films were fabricated by a 200 MPa pressure rolling compression process. Subsequently, the single annealed graphene film was annealed at 2850 °C for 1 h again. Finally, the GAF was obtained after being rolled and compressed at a pressure of 200 MPa.

Figure 1a depicts the photograph of a GAF, showing the metallic texture and flexibility of GAF, which can be attributed to high-temperature treatment. After annealing at 2850 °C for 2 h under an argon atmosphere, defects inside the GAF healed, and the graphitization degree intensely increased, as demonstrated in the Raman spectra of GAF in Figure 1b, in which the peak of the D band at around 1350 cm^{-1} is quite weak, while the peak of the G band is strong and intense.[31] The XRD pattern further validates the high crystallization degree of GAF (Figure 1c), where the sharp and intense (0 0 2) peak at around 26.5° implies a highly oriented stacked graphitization structure and an interplanar spacing of 0.34 nm. Figure 1d shows the surficial SEM image of GAF. Multiple wrinkles on the GAF surface play an important part in improving the flexibility of GAF.[32] Figure 1e is the cross-sectional SEM image of a GAF, showing a thickness of 25 μm. Moreover, by the focus ion beam technique, we have demonstrated that the interplanar spacing of the GAF (0 0 2) interplanar is 0.34 nm (Figure 1f), which is consistent with the calculated results of XRD patterns, further verifying the high quality of our GAFs. In this work, the conductivity of the GAF that we used for the antenna array is 1.1×10^6 S/m, which has been confirmed to have no significant impact on the antenna performance in our previous work.[33]

3. RESULTS AND DISCUSSION

3.1. Design of the GAF Antenna Arrays. The magneto-electric dipole-formed antennas have many advantages, such as wide band, stable gain, and low cross-polarization. Based on

https://doi.org/10.1021/acsami.3c10732
ACS Appl. Mater. Interfaces XXXX, XXX, XXX−XXX

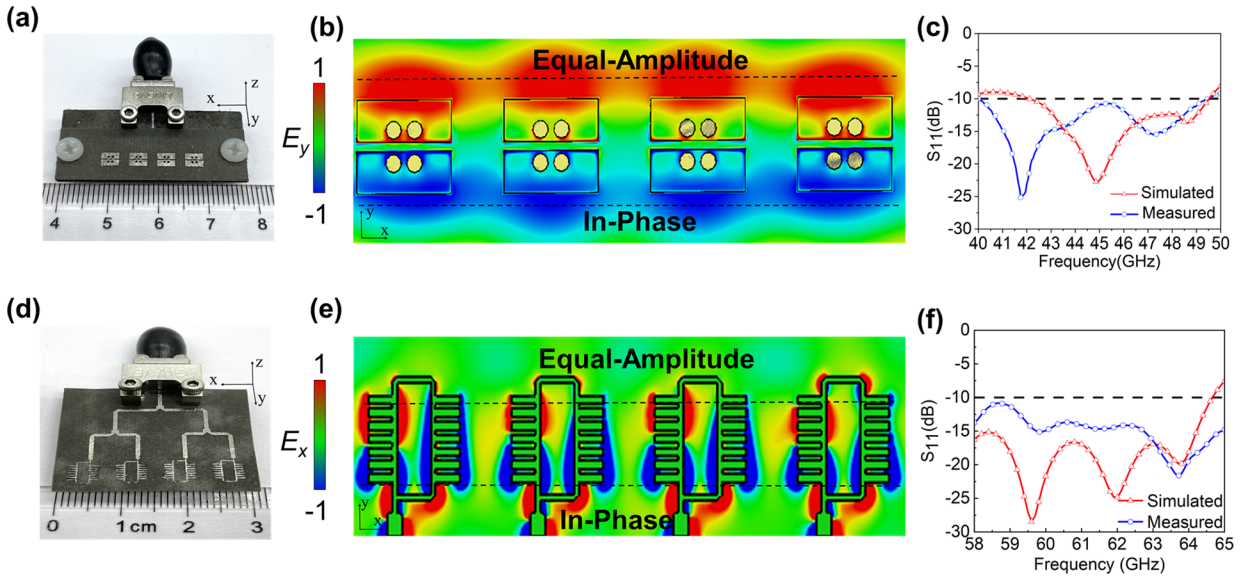

Figure 2. (a) Photographs of the magnetoelectric dipole antenna array; (b) electric field distributions of the magnetoelectric dipole antenna array at 45 GHz; (c) simulated and measured S-parameters of the magnetoelectric dipole antenna array; (d) photographs of the microstrip discontinuous radiation antenna array; (e) electric field distributions of the microstrip discontinuous radiation antenna array at 60 GHz; (f) simulated and measured S-parameters of the microstrip discontinuous radiation antenna array.

this, we proposed a new symmetric magnetoelectric dipole antenna with a top and bottom symmetric four-layer dielectric substrate (shown in Figure S1). In order to reduce the dielectric loss at 45 GHz, the substrate adopts a Rogers RT/Duriod 5880 commercial high-frequency laminate with thicknesses of 0.254 and 0.787 mm, dielectric constant of 2.2, and a loss tangent of 0.0009. Further, we used the LPKF S-Series laser engraver with a fabrication tolerance of 15 μm, which is 0.003% of the antenna's operating wavelength, ensuring the good performance of the antenna. The resonance frequency of the antenna can be adapted by the antenna patch of length L and width W, as indicated in Figure S2a,b. We note that as L increases, the resonance intensity of the antenna first increases and then decreases, and the resonance frequency moves from a high frequency to low frequency. As the width W increases, the resonance intensity of the antenna changes little, and the single resonance frequency decreases from a high to low frequency. As illustrated in Figure S2c, the GAF magnetoelectric dipole antenna element has a simulated bandwidth of 40−49.8 GHz and a peak realized gain of 5.27 dBi. The 3D radiation pattern of the antenna is shown in Figure S3. It indicates that the GAF magnetoelectric dipole antenna has a bidirectional symmetric beam. The photos of the GAF magnetoelectric dipole antenna, S-parameters, and realized gain are demonstrated in Figures S4 and S5. We can note that the bandwidth of the GAF antenna covers 40−50 GHz. Figure S6 shows the antenna element simulation and measured normalized radiation patterns at 43.5, 45, and 47 GHz. We noticed that the radiation patterns are symmetric and stable over the entire working band. The half-power beamwidths of the GAF antenna array in the *yoz*-plane (E-plane) and *xoz*-plane (H-plane) are 105° and 55°, respectively.

High gain is a widespread requirement for millimeter-wave antennas. According to the proposed 45 GHz GAF antenna element, a 1 × 4 GAF millimeter-wave short-range wireless communication antenna array is developed to improve the antenna radiation gain and directionality. The feeding network is important to the performance of the antenna array since it controls the amplitude and phase distribution of antenna elements and ultimately affects the synthetic radiation pattern. T-junction is the most common and the simplest type of power divider, which can be fabricated by transmission lines such as waveguide, coaxial, stripline, or microstrip. As shown in Figure S7a, three stripline T-junction power dividers are used here to distribute the power of the input port (Port 1) to the four output ports (Ports 2−5) with the same amplitude and phase. Figure S7b,c depicts the simulated S-parameters and phases of the GAF stripline feeding network. The reflection coefficient of the input port 1 is less than −10 dB for the whole operating frequency band. The four output ports have equal transmission coefficients (|S21|−|S51|), which indicate that the power at the input ports is equally distributed to port 5. In addition, as illustrated in Figure S7c, the four output ports have identical phases.

Figure 2a illustrates the photographs of the GAF magnetoelectric dipole antenna array. A 2.4 mm solderless coaxial connector is used for excitation. Figure 2b demonstrates the electric field distributions of the magnetoelectric dipole antenna array at 45 GHz, simulated by CST Studio. It can be concluded that the four elements have equivalent amplitudes and identical phases, which mean that the power divider network of the antenna array has good performance. Figure 2c depicts the simulated and measured S-parameters of the magnetoelectric dipole antenna array. The simulated bandwidth of 42−49.5 GHz is in agreement with the measured bandwidth.

For 60 GHz, which is the typical band for millimeter-wave communication, we proposed an easily processed GAF microstrip discontinuous radiation antenna. Figure S9a,b shows the structure of a GAF-based 60 GHz microstrip discontinuous radiation antenna element. The microstrip antenna has the benefits of cheap cost, easy processing, low profile, and excellent radiation performance. To reduce the dielectric loss at 60 GHz, the substrate adopts a Rogers RT/Duriod 5880 commercial high-frequency laminate with the same parameters. The antenna utilizes the fringing open

https://doi.org/10.1021/acsami.3c10732
ACS Appl. Mater. Interfaces XXXX, XXX, XXX−XXX

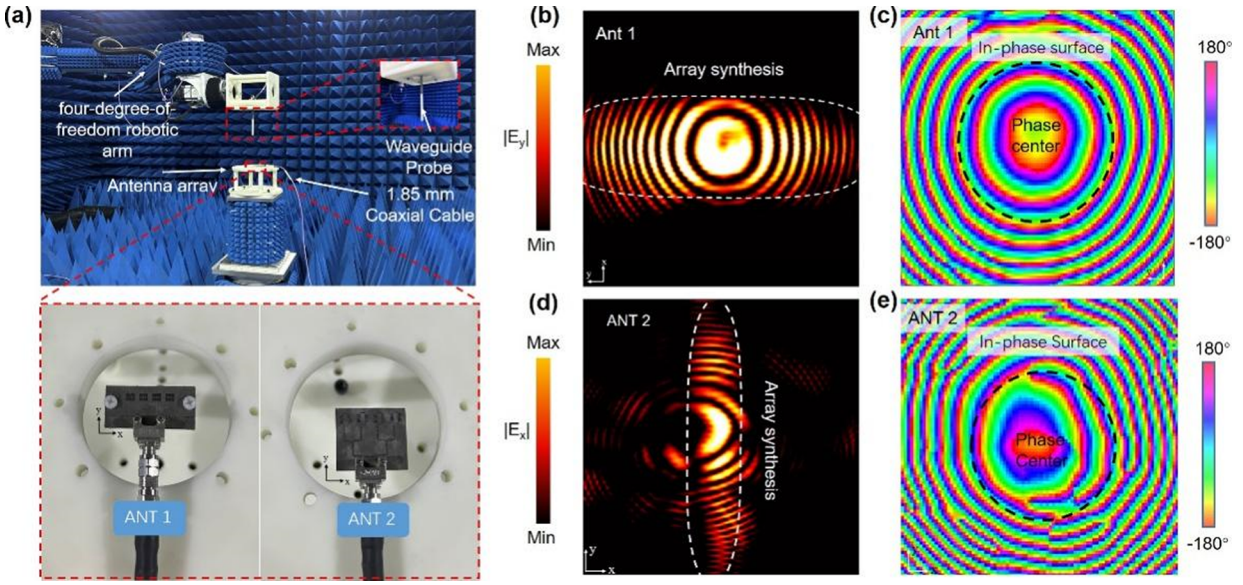

Figure 3. (a) Experimental setup for the near-field measurement of the proposed antenna array; (b) measured near-field electric field magnitude (|*Ey*|) distributions of the magnetoelectric dipole antenna array at 45 GHz; (c) measured near-field electric field phase distributions of the magnetoelectric dipole antenna array at 45 GHz; (d) measured near-field electric field magnitude (|*Ex*|) distributions of the microstrip discontinuous radiation antenna array at 60 GHz; (e) measured near-field electric field phase distributions of the microstrip discontinuous radiation antenna array at 60 GHz.

microstrip line for radiation and also is fabricated by an LPKF S-Series laser engraver. By adding a number of open lines, the antenna can achieve a higher gain. In addition, the length of the feeder microstrip line (*FL*) was purposely extended to reduce the influence of the connector on the radiation pattern during the test.

The GAF discontinuous radiation antenna element structure was also modeled and simulated by CST Studio. The variation of the antenna resonance frequency with the length *DL* and distance *RW* of the open line is shown in Figure S10a,b. We can conclude that the length *DL* has a strong correlation with the resonance depth and resonance frequency of the GAF antenna element. When the open line distance *RW* is increased from 1.6 to 1.8 mm, the resonance frequency of the antenna gradually moves to a lower frequency. Figure S10c shows the simulated S-parameters and simulated gain of the optimized GAF antenna element. The GAF antenna has a bandwidth of 59−64 GHz with a stable gain over the entire frequency band. Figure S11 shows the simulated 3D radiation pattern of the GAF microstrip discontinuous radiation antenna, which proves that the GAF antenna radiates effectively, and the maximum radiation direction is the normal direction of antenna plane. The beamwidth of the antenna in the *xoz*-plane (H-plane) is 57°, which is wider than 39° in the *yoz*-plane (E-plane). The radiation of the antenna in the side and backward directions is small, which is beneficial to the directional transmission of signals in millimeter-wave, short-range wireless communications. The digital photograph of the GAF microstrip antenna element is shown in Figure S12, with the measured reflection coefficient and realized gain shown in Figure S13. The results indicate that the measured impedance bandwidth of 58−65 GHz is basically in agreement with the simulated results, with a peak realized gain of 10.96 dBi. Figure S14 demonstrates the simulated and measured normalized radiation patterns of the 60 GHz antenna elements at 59, 60, and 64 GHz. We note that the simulated and measured results of the antenna are in good agreement. The measured half-power beam width of the GAF antenna array in the *xoz*-plane (E-plane) and *yoz*-plane (H-plane) are 40° and 60°, respectively.

In order to obtain a higher gain and directionality, we further proposed an array based on the above 60 GHz microstrip discontinuous radiation antenna elements. According to the structural characteristics of the microstrip antenna element, the feeding network is designed utilizing a microstrip line, as depicted in Figure S15a. Figure S15b,c plots the simulated S-parameters and phases of the GAF microstrip feeding network. The reflection coefficient of input port 1 is less than −10 dB in the whole operating frequency band. All the output ports have similar transmission coefficients (|S21|−|S51|) which indicates that the power of the input port is equally distributed to the four output ports. In addition, the four output ports have identical phases, as shown in Figure S15c.

As illustrated in Figure 2d, the GAF 60 GHz antenna array consists of a microstrip feeding network and four antenna elements connecting a 1.85 mm coaxial connector for feeding. Figure 2e shows the electric field distributions of the microstrip discontinuous radiation antenna array at 60 GHz. It can be concluded that the four elements have equal amplitude and are in phase, which mean that the power divider can equally distribute the power of the input port to the four elements with the same phase. As shown in Figure 2f, the simulated bandwidth is from 58 to 64.6 GHz, and the measured result is from 58 to 65 GHz. The results between the measurement and simulation have good agreement.

3.2. Near-Field and Far-Field Antenna Arrays. Figure 3a shows the experimental setup for the near-field electric field measurement. The experimental setup consists of a vector network analyzer (VNA, Ceyear 3672), a three-dimensional robotic arm, and a waveguide probe antenna. The GAF antenna is placed on a fixed table. The probe antenna is placed on the robotic arm which is contorted by a computer. The probe antenna is placed at 100 mm above the sample and moved to scan the electric field distributions, with the scanning step of 2 mm. The electric field amplitude and phase data were

https://doi.org/10.1021/acsami.3c10732
ACS Appl. Mater. Interfaces XXXX, XXX, XXX−XXX

collected and recorded with a network analyzer. The whole measurement of electric field distributions in this work was carried out in an anechoic chamber. The simulated and measured near-field electric field magnitude distributions (|*Ey*|) of the magnetoelectric dipole antenna array at 45 GHz are shown in Figures S17a and 3b, proving that the radiation power is concentrated on the center of the antenna array due to the array synthesis. Figures S17b and 3c depict the simulated and measured near-field electric field phase distributions of the 45 GHz magnetoelectric dipole antenna array. It can be seen that the phase center is the geometrical center of the antenna array, illustrating that the antenna array is equivalent to a point source antenna and that the radiation wave spread transmits from the antenna center to the space. Correspondingly, Figures S17c and 3d show the simulated and measured near-field electric field magnitude (|*Ex*|) distributions of the microstrip discontinuous radiation antenna array. We note that the energy is concentrated on the center of the antenna array, which is in agreement with the results of Figures S17a and 3b. Figures S17d and 3e plot the simulated and measured near-field electric field phase distributions of the 60 GHz microstrip discontinuous radiation antenna array. The phase center also coincides with the antenna array geometrical center, proving that the antenna array is equivalent to a point source antenna.

Figure 4a shows the experimental verification of the antenna radiation patterns. The devices consist of a vector network analyzer, two sliding rails for controlling the position of the detector, a stepping motor for controlling the polarization direction, and a standard horn antenna as a detector. The detector was fixed 1 m from the antenna array. The antenna array was placed on a rotating platform and rotated in a step of 1°. The electric magnitude data were recorded by the network analyzer. The whole measurement was also carried out in the anechoic chamber to reduce the impact of environmental interference. Figure 4b shows the simulated and measured realized gain of the 45 GHz magnetoelectric dipole antenna array. The simulated peak realized gain is 12.39 dBi, and the measured gain is 11.8 dBi. Figures 4c and S18 show the simulated and measured *xoz*-plane (H-plane)- and *yoz*-plane (E-plane)-normalized far-field radiation patterns of the magnetoelectric dipole antenna array. The measurements agree well with the simulation results, and the half-power beam widths of the E-plane and H-plane are 47° and 16°, respectively. Furthermore, the proposed antenna array has a symmetrical beam, which is suitable for the bidirectional short-range wireless communication. Figure 4d displays the realized gain of the microstrip discontinuous radiation antenna array. The measured peak realized gain of the antenna array is 13.92 dBi, which agrees with the simulated result of 14.49 dBi. Figures 4e and S19 display the simulated and measured *xoz*-plane (E-plane) and *yoz*-plane (H-plane) normalized radiation patterns of the microstrip discontinuous radiation antenna array. The simulated and measured results are in good agreement. The measured half-power beam widths of the GAF antenna array in the *xoz*-plane and *yoz*-plane are 9° and 70°, respectively. Comparing the radiation patterns of the E-plane and H-plane of the antenna array with different frequencies, the radiation characteristics of the array antenna are observed to be stable in the entire operating frequency band.

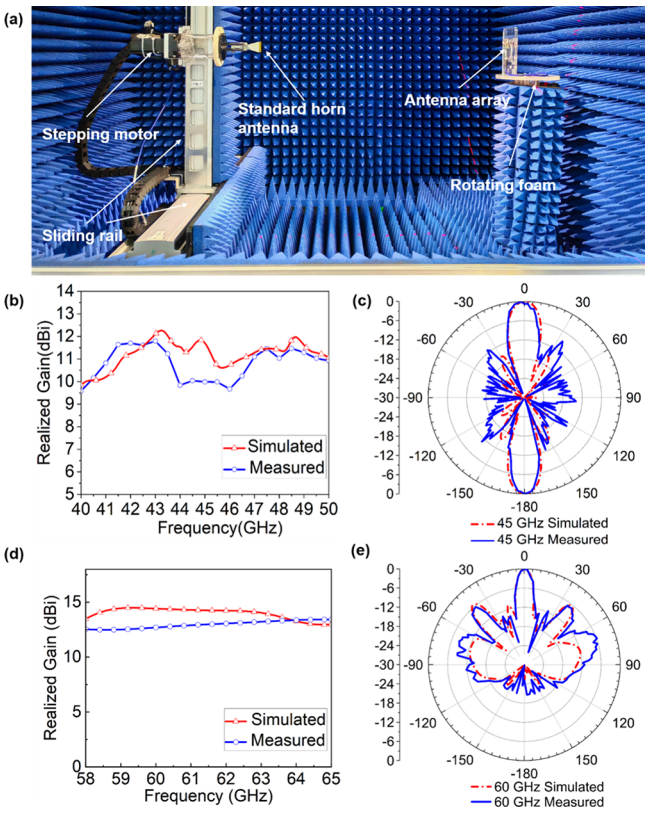

Figure 4. (a) Experimental verification devices of the antenna radiation patterns; (b) realized gains of the magnetoelectric dipole antenna array; (c) simulated and measured *xoz*-plane-normalized far-field radiation patterns of the magnetoelectric dipole antenna array; (d) peak realized gains of the microstrip discontinuous radiation antenna array; (e) simulated and measured *xoz*-plane-normalized far-field radiation patterns of the microstrip discontinuous radiation antenna array.

4. APPLICATIONS AND DISCUSSION

The two proposed antenna arrays show good performance in 45 and 60 GHz short-range wireless communication bands. To validate the application prospects in indoor wireless communication of the proposed antenna arrays, a sample wireless transceiver system is built to perform indoor signal coverage division experiments. First, we demonstrate the application scenario of two antenna arrays in a typical indoor environment, where the antennas are placed in a conference room to communicate with computers, printers, and so forth (in Figure 5a). Figures 5b and S20 illustrate the experimental validation of the 45 GHz magnetoelectric dipole antenna array and the 60 GHz microstrip discontinuous radiation antenna array measured by a vector network analyzer. To eliminate the loss of coaxial cable, a low-noise amplifier is used, and the output power from the VNA is adopted to −10 dBm. The experiment involves three steps: first, the distance between the transmitter and receiver is set at 10 cm and marked as normalization; second, the distance was changed at 30 cm intervals, and the data of S21 were saved by the VNA. Third, the receiving antenna was moved outside to measure the signal through the wall. Figure 5c,d displays the received power of the horn antenna. The results indicate that in a 4 × 5 m^2 conference room, the signal drops slowly to −27 dB (45 GHz) and −30 dB (60 GHz) at the rate of 0.064 and 0.071 dB/cm, respectively, proving that the signal can cover the

https://doi.org/10.1021/acsami.3c10732
ACS Appl. Mater. Interfaces XXXX, XXX, XXX−XXX

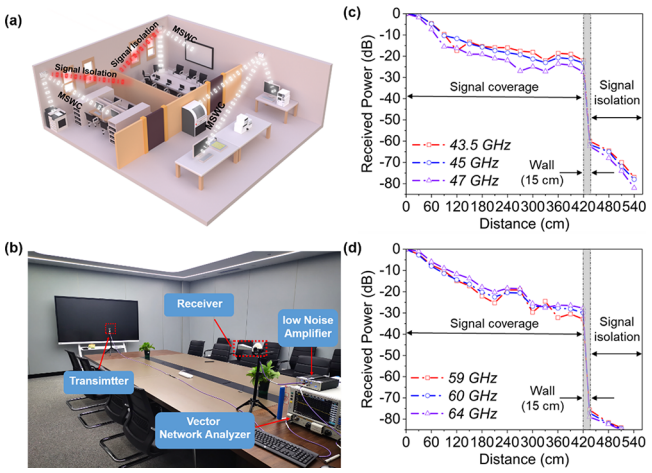

Figure 5. (a) Illustrative scenario for the proposed short-range wireless communication in a typical indoor environment; (b) experimental signal transmission of the proposed antenna arrays; and the received power of (c) 45 GHz magnetoelectric dipole antenna array and (d) 60 GHz microstrip discontinuous radiation antenna array.

entire room. When transmitted through a 15 cm thick wall, the signal drops steeply to −60 dB and −77 dB at 2.3 and 3.13 dB/cm, respectively, which is more than 35 times the difference in indoor results. We can conclude that the two proposed antenna arrays can achieve the signal coverage of the entire room and restrain the signal leakage out of the room, which can achieve high-speed indoor wireless communication while reducing signal interference and improving information confidentiality.

5. CONCLUSIONS

In conclusion, this work demonstrates two millimeter-wave short-range wireless communication antenna arrays for the IEEE 802.11aj and 802.11ad standards based on graphene-assembled films. For the 45 GHz band, the proposed graphene-assembled film magnetoelectric dipole antenna array has a wide operating bandwidth of 40−49.5 GHz and a bidirectional symmetric beam with the peak realized gain of 11.8 dBi. For the 60 GHz band, the proposed graphene-assembled film microstrip discontinuous radiation antenna array operates at 59−64 GHz with the peak realized gain of 14.92 dBi. To verify the performance of the proposed antenna arrays in a short-range wireless communication, we construct a wireless communication scheme for signal transfer in a conference room. The results indicate that the signals of the two proposed antenna arrays drop slowly in the room and drop steeply after transmission through the walls, with a difference of more than 35 times between the two drop rates, providing signal coverage of the entire room while restraining signal leakage, which improves the security of the information. This research shows promising applications for high-capacity, low-latency, and high-density access required for future millimeter-wave, short-range wireless communications. Meanwhile, it confirms the great application value of graphene-assembled films in a high-frequency microwave field.

■ ASSOCIATED CONTENT

Supporting Information

The Supporting Information is available free of charge at https://pubs.acs.org/doi/10.1021/acsami.3c10732.

Antenna elements' simulated and measured results; simulated results of antenna arrays; and experimental signal transmission through the wall (PDF)

■ AUTHOR INFORMATION

Corresponding Authors

Rongguo Song − *Hubei Engineering Research Center of RF-Microwave Technology and Application, Wuhan University of Technology, Wuhan 430070, China; Air Force Early Warning Academy, Wuhan 430019, China*; Email: rongguo_song@whut.edu.cn

Haoran Zu − *Hubei Engineering Research Center of RF-Microwave Technology and Application, Wuhan University of Technology, Wuhan 430070, China; School of Information Engineering, Wuhan University of Technology, Wuhan 430070, China*; Email: zuhr@whut.edu.cn

Daping He − *Hubei Engineering Research Center of RF-Microwave Technology and Application, Wuhan University of Technology, Wuhan 430070, China*; orcid.org/0000-0002-0284-4990; Email: hedaping@whut.edu.cn

Authors

Yitong Xin − *Hubei Engineering Research Center of RF-Microwave Technology and Application, Wuhan University of Technology, Wuhan 430070, China*

Shaoqiu Jiang − *Hubei Engineering Research Center of RF-Microwave Technology and Application, Wuhan University of Technology, Wuhan 430070, China*

Huaqiang Fu − *School of Materials Science and Engineering, Wuhan University of Technology, Wuhan 430070, China*

Wei Qian − *Hubei Engineering Research Center of RF-Microwave Technology and Application, Wuhan University of Technology, Wuhan 430070, China*

Dong Ye − *Hubei Engineering Research Center of RF-Microwave Technology and Application, Wuhan University of Technology, Wuhan 430070, China*

Jiannan Guo − *Hubei Engineering Research Center of RF-Microwave Technology and Application, Wuhan University of Technology, Wuhan 430070, China*

Zixin Zhang − *School of Materials Science and Engineering, Wuhan University of Technology, Wuhan 430070, China*

Complete contact information is available at: https://pubs.acs.org/10.1021/acsami.3c10732

Author Contributions

⊥Y.X. and R.S. contributed equally to this work

Notes

The authors declare no competing financial interest.

■ ACKNOWLEDGMENTS

The authors acknowledge financial support from the National Natural Science Foundation of China (51672204 and 51701146), Wuhan Application Foundation Frontier Project (grant no. 2020020601012220), and the Fundamental Research Funds for the Central Universities (WUT: 205209016 and 2020IB005). We also thank the Analytical and Testing Center of Wuhan University of Technology for performing various characterizations and measurements.

REFERENCES

(1) Pyattaev, A.; Johnsson, K.; Andreev, S.; Koucheryavy, Y. Communication Challenges in High-density Deployments of Wearable Wireless Devices. *IEEE Wireless Commun.* **2015**, *22* (1), 12−18.

(2) Ding, J.; Nemati, M.; Ranaweera, C.; Choi, J. IoT Connectivity Technologies and Applications: A Survey. *IEEE Access* **2020**, *8*, 67646−67673.

(3) Qiao, X.; Ren, P.; Dustdar, S.; Liu, L.; Ma, H.; Chen, J. Web AR: A Promising Future for Mobile Augmented Reality—State of the Art, Challenges, and Insights. *Proc. IEEE* **2019**, *107* (4), 651−666.

(4) Hong, W.; Wang, H.; Chen, J.; Zhang, N.; Zhang, Y.; Yang, G.; Yan, P.; Yu, C.; Chen, Z.; Liang, W.; Zhu, F. Recent Advances in Q-LINKPAN/IEEE 802.11aj (45 GHz) Millimeter Wave Communication Technologies. In *2013 Asia-Pacific Microwave Conference Proceedings (APMC)*, 2013; pp 227−229.

(5) Gebreyohannes, F. T.; Frappé, A.; Kaiser, A. A ConFigureurable Transmitter Architecture for IEEE 802.11ac and 802.11ad Standards. *IEEE Trans. Circuits Syst. II: Express Briefs* **2016**, *63* (1), 9−13.

(6) Kong, L.; Khan, M. K.; Wu, F.; Chen, G.; Zeng, P. Millimeter-Wave Wireless Communications for IoT-Cloud Supported Autonomous Vehicles: Overview, Design, and Challenges. *IEEE Commun. Mag.* **2017**, *55* (1), 62−68.

(7) Gan, Z.; Tu, Z.-H.; Xie, Z.-M.; Chu, Q.-X.; Yao, Y. Compact Wideband Circularly Polarized Microstrip Antenna Array for 45 GHz Application. *IEEE Trans. Antennas Propag.* **2018**, *66* (11), 6388−6392.

(8) Yang, T. Y.; Hong, W.; Zhang, Y. An SICL-Excited Wideband Circularly Polarized Cavity-Backed Patch Antenna for IEEE 802.11aj (45 GHz) Applications. *IEEE Antennas Wireless Propag. Lett.* **2016**, *15*, 1265−1268.

(9) Zu, H.; Wu, B.; Chen, B.; Li, W.; Su, T.; Liu, Y.; et al. Optically and Radiofrequency-transparent Metadevices based on Quasi-one-dimensional Surface Plasmon Polariton Structures. *Nat. Electron.* **2023**, *6*, 525−533.

(10) Al-Alem, Y.; Kishk, A. A. Low-Cost High-Gain Superstrate Antenna Array for 5G Applications. *IEEE Antennas Wireless Propag. Lett.* **2020**, *19* (11), 1920−1923.

(11) Jang, T. H.; Han, Y. H.; Kim, J.; Park, C. S. 60 GHz Wideband Low-Profile Circularly Polarized Patch Antenna With an Asymmetric Inset. *IEEE Antennas Wireless Propag. Lett.* **2020**, *19* (1), 44−48.

(12) Awasthi, A. K.; Li, J.; Koh, L.; Ogunseitan, O. A. Circular Economy and Electronic Waste. *Nat. Electron.* **2019**, *2* (3), 86−89.

(13) Nithya, R.; Sivasankari, C.; Thirunavukkarasu, A. Electronic Waste Generation, Regulation and Metal Recovery: A Review. *Environ. Chem. Lett.* **2021**, *19* (2), 1347−1368.

(14) Trzebiatowski, K.; Rzymowski, M.; Kulas, L.; Nyka, K. Simple 60 GHz Switched Beam Antenna for 5G Millimeter-Wave Applications. *IEEE Antennas Wireless Propag. Lett.* **2021**, *20*, 38−42.

(15) Rebhi, L.; Krstic, B.; Boutemedjet, A.; Totovski, L.; Vucetic, N.; Milutinovic, M.; Rezgui, N. Fatigue Fracture Analysis of an ADF Antenna in a Military Aircraft. *Eng. Failure Anal.* **2018**, *90*, 476−488.

(16) Wang, Y.; Yan, C.; Cheng, S.-Y.; Xu, Z.-Q.; Sun, X.; Xu, Y.-H.; Chen, J.-J.; Jiang, Z.; Liang, K.; Feng, Z.-S. Flexible RFID Tag Metal Antenna on Paper-Based Substrate by Inkjet Printing Technology. *Adv. Funct. Mater.* **2019**, *29* (29), No. 1902579.

(17) Singh, V.; Joung, D.; Zhai, L.; Das, S.; Khondaker, S. I.; Seal, S. Graphene Based Materials: Past, Present and Future. *Prog. Mater. Sci.* **2011**, *56* (8), 1178−1271.

(18) Pan, K.; Fan, Y.; Leng, T.; Li, J.; Xin, Z.; Zhang, J.; Hao, L.; Gallop, J.; Novoselov, K. S.; Hu, Z. Sustainable Production of Highly Conductive Multilayer Graphene Ink for Wireless Connectivity and IoT Applications. *Nat. Commun.* **2018**, *9* (1), 5197.

(19) He, P.; Cao, J.; Ding, H.; Liu, C.; Neilson, J.; Li, Z.; Kinloch, I. A.; Derby, B. Screen-Printing of a Highly Conductive Graphene Ink for Flexible Printed Electronics. *ACS Appl. Mater. Interfaces* **2019**, *11* (35), 32225−32234.

(20) Wang, W.; Ma, C.; Zhang, X.; Shen, J.; Hanagata, N.; Huangfu, J.; Xu, M. High-Performance Printable 2.4 GHz Graphene-based Antenna Using Water-transferring Technology. *Sci. Technol. Adv. Mater.* **2019**, *20*, 870−875.

(21) Huang, X.; Leng, T.; Zhang, X.; et al. Binder-free Highly Conductive Graphene Laminate for Low Cost Printed Radio Frequency Applications. *Appl. Phys. Lett.* **2015**, *106* (20), 203105.

(22) Sa Don, S. N.; Jamaluddin, M. H.; Kamarudin, M. R.; Ahmad, F.; Yamada, Y.; Kamardin, K.; Idris, I. H. Analysis of Graphene Antenna Properties for 5G Applications. *Sensors* **2019**, *19* (22), 4835 DOI: 10.3390/s19224835.

(23) Sa'Don, S.; Jamaluddin, M. H.; Kamarudin, M. R.; Ahmad, F. A 5G Graphene Antenna Produced by Screen Printing Method. *Indones. J. Electr. Eng. Comput. Sci.* **2019**, *15*, 950−955.

(24) Song, R.; Wang, Q.; Mao, B.; Wang, Z.; Tang, D.; Zhang, B.; Zhang, J.; Liu, C.; He, D.; Wu, Z.; Mu, S. Flexible Graphite Films With High Conductivity for Radio-frequency Antennas. *Carbon* **2018**, *130*, 164−169.

(25) Luo, K.; Zu, H.; Song, R.; Xin, Y.; Guo, J.; Ye, D.; Xu, M.; Huang, G.; He, D. An Anisotropic Broadband Coding Metasurface Based on Ultralight Graphene-Assembled Film Microw. *Opt. Technol. Lett.* **2023**, *65*, 3211−3220.

(26) Hu, Z.; Xiao, Z.; Jiang, S.; Song, R.; He, D. A Dual-Band Conformal Antenna Based on Highly Conductive Graphene-Assembled Films for 5G WLAN Applications. *Materials* **2021**, *14*, 5087.

(27) Song, R.; Jiang, S.; Hu, Z.; Fan, C.; Li, P.; Ge, Q.; Mao, B.; He, D. Ultra-high Conductive Graphene Assembled Film For Millimeter Wave Electromagnetic Protection. *Sci. Bull.* **2022**, *67* (11), 1122−1125.

(28) Song, R.; Zhao, X.; Wang, Z.; Fu, H.; Han, K.; Qian, W.; Wang, S.; Shen, J.; Mao, B.; He, D. Sandwiched Graphene Clad Laminate: A Binder-Free Flexible Printed Circuit Board for 5G Antenna Application. *Adv. Eng. Mater.* **2020**, *22* (10), No. 2000451.

(29) Song, R.; Wang, Z.; Zu, H.; Chen, Q.; Mao, B.; Wu, Z.; He, D. Wideband and low sidelobe graphene antenna array for 5G applications. *Sci. Bull.* **2021**, *66* (2), 103−106.

(30) Jiang, S.; Song, R.; Hu, Z.; Xin, Y.; Huang, G.; He, D. Millimeter wave phased array antenna based on highly conductive graphene-assembled film for 5G applications. *Carbon* **2022**, *196*, 493−498.

(31) Ferrari, A.; Robertson, J.; Reich, S.; Thomsen, C. Raman spectroscopy of graphite. *Philos. Trans. R. Soc., A* **2004**, *362* (1824), 2271−2288.

(32) Peng, L.; Xu, Z.; Liu, Z.; Guo, Y.; Li, P.; Gao, C. Ultrahigh Thermal Conductive yet Superflexible Graphene Films. *Adv. Mater.* **2017**, *29* (27), No. 1700589.

(33) Song, R.; Mao, B.; Wang, Z.; Hui, Y.; Zhang, N.; Fang, R.; Zhang, J.; Wu, Y.; Ge, Q.; Novoselov, K.; He, D. Comparison of Copper and Graphene Assembled Filmsin 5G Wireless Communication and THz Electromagnetic-Interference Shielding. *Proc. Natl. Acad. Sci. U. S. A.* **2023**, *120* (9), No. e2209807120.

https://doi.org/10.1021/acsami.3c10732
ACS Appl. Mater. Interfaces XXXX, XXX, XXX−XXX